CHARACTERIZATION OF THE FMT-2 DISCHARGE CATHODE PLUME

George J. Williams, Jr. , Timothy B. Smith*, Travis A. Patrick*, and
Alec D. Gallimore†
Plasmadynamics and Electric Propulsion Laboratory
Department of Aerospace Engineering
The University of Michigan
1919 Green Rd., Ann Arbor, MI 48105, USA

Abstract

Laser-induced fluorescence and emission spectroscopy were used to interrogate the plasma downstream of the discharge cathode in the FMT-2 ion engine. Ion velocities consistent with a potential hill approximately 0.75 cm downstream of the unkeepered orifice were observed at higher powers. The high energy tail, discharge voltage oscillations, and the concentration of Xe III may collectively contribute to the erosion observed in NSTAR wear tests.

Introduction

Ion thrusters are being scaled to different powers and operating conditions for space flight applications. A baseline for this scaling is the NASA Solar Electric Propulsion Technology Readiness (NSTAR) 30 cm ion thruster. Several wear-tests have been conducted to demonstrate long duration operation and life-limiting phenomena. One of the potential failure mechanisms identified during these tests was erosion of the discharge cathode assembly.

Severe erosion of the outer edge of the orifice plate, W at 145 μm/khr; of the tip of the cathode tube, Mo at 280 μm/khr; and of the heater coil outer sheath, Ta, were observed in the 2000 hr development wear-test.[1] A keeper electrode was introduced as an engineering solution, and, after a subsequent 1000 hr wear-test the observed erosion was reduced to less than 3 μm/khr.[2] This is significantly below the estimated acceptable threshold of 64 μm/khr based on the location of the electron beam weld between the cathode tube and the orifice plate. However, during an 8200 hr wear-test the keeper orifice plate was observed to erode at roughly 60 μ/khr which was acceptable given the 8000 hr lifetime, keeper orifice plate geometry, and 2.3 kW operating condition.[3] It has been suggested that higher powers and longer periods of operation can be accommodated by thickening the orifice plates.[4] However, recent developments in cathode assembly design may not make this a feasible option.[5,6]

The source of the high-energy ions causing the erosion is largely unknown. Ray-tracing after the 2000 hr test indicated the source of the ions was located between 1 and 11 mm downstream of the orifice plate. The potential-hill phenomenon, which has been postulated as the source of high-energy ions eroding downstream cathode-potential surfaces, is the leading explanation.[7] However, sheath effects may account for the erosion pattern and plasma oscillations might also yield the high-energy ions required for the erosion.

Laser-induced fluorescence (LIF) and emission spectroscopy were employed in this investigation to measure the Xe II velocity distribution and species concentrations near the exit of the discharge cathode, respectively. These investigations were conducted at the Plasmadynamics and Electric Propulsion Laboratory (PEPL) at the University of Michigan.

Apparatus and Procedure

Thruster

The functional model thrusters (FMTs) were the immediate predecessor to the NSTAR engineering model thrusters (EMTs) which preceded the NSTAR flight thrusters. The FMTs differed principally from the EMTs in their soft aluminum construction. FMT-2 was modified at the NASA Glenn Research Center (GRC) to ensure a discharge cathode environment identical to EMT-1 which was the subject of the 2000 hr wear-test and to provide optical access to the discharge chamber. The magnetic field, discharge cathode assembly (DCA), and geometry of the discharge chamber were identical to EMT-1's. The quartz windows replaced roughly twenty percent of the anode surface as shown in Fig. 1 and appear to have a negligible impact on discharge chamber and thruster performance. The thruster has been operated over the entire NSTAR power throttling range at both GRC and at PEPL. Performance of the thruster is comparable to the engineering and flight model thrusters. The thruster was operated using a modified Skit-Pac provided by NASA GRC.

---

* Graduate Student

The DCA was the same as that used during the second segment of the 2000 hr wear test. As in this test, but unlike all subsequent EMT operation, the DCA did not incorporate a keeper electrode.

Vacuum Facility

This investigation was performed in the 6 m x 9 m large vacuum test facility (LVTF) at PEPL. Four CVI Model TM-1200 Re-Entrant Cryopumps provided a combined pumping speed of 140,000 l/s on xenon with a base pressure of less than $2\ 10^{-7}$ Torr. The back pressure during 2.3 kW operation was roughly $3\ 10^{-6}$ Torr corrected for xenon.

Xenon flow was controlled to the thruster using a dedicated propellant feed system provided by NASA GRC. The flow rates were periodically calibrated using a bubble flow meter between tests. No significant variation was observed.

The FMT was mounted on a two-axis positioning system. The two translation stages were controlled and monitored via a computer which provided repeatability of measurements over an extended period. Resolution was on the order of 0.025 cm for both stages.

A 2 m by 2.5 m louvered graphite panel-beam dump protected windows downstream of the thruster and suppressed back sputtering. The panels were located roughly 4 m downstream of the thruster.

Laser and Optics

An argon-ion pumped Coherent dye laser (899-29 model) was used with Rhodamine-6G dye. Xe I at 582 nm and Xe II at 605 nm were interrogated using a multiple-beam technique[8] wherein three and four-beam LIF is performed. The three-beam LIF measured all three velocity components simultaneously. A second axial beam was used in the four-beam technique to increase the resolution of the axial velocity measurement at higher thruster powers. Both techniques used a Hamamatsu reference cell to provide a zero velocity datum. The laser was typically scanned over a 0.01 nm interval in 0.061 pm increments. The beams were delivered to the thruster in a manner identical to that used in previous Hall thruster interrogations.[8] Alignment was facilitated by a wire crosshair on the side of the FMT plasma screen.

Induced and natural fluorescence data were collected using Spex 500 M and Spex H10 monochromators fitted with Hamamatsu 928 PMTs. Both fluorescence signals were controlled and recorded via computers. The Spex 500 M monochromator's slits were set to 50 μm. Because of a 2x magnification, the effective spot size at the focus of the collection lens was 25 μm. The bi-conical sample volume in the cathode plume was roughly 0.5 cm long and 0.1 cm in diameter at its ends. Measurements taken far downstream of the cathode at low power indicate that the ambient plasma outside of the cathode plume contributes less than five percent to the natural fluorescence signal. The laser delivery and signal collection optics are shown in Fig. 2.

Several rapid (~ 10 s) scans were taken at each data point. The rapid scans prevented long lock-in time constants from artificially shifting the fluorescence spectra to lower frequencies which would falsely indicate lower velocities. These scans were then ensemble averaged to remove the noise.

Theory

Laser-Induced Fluorescence

The absorbing neutral xenon, Xe I, or singly ionized xenon, Xe II, will "see" the wavelength of the incoming laser photons shifted by the relative motion of the particle in the direction of the photon.

$$\Delta \nu = \nu_0 \left(v_i / c \right) \qquad (1)$$

The velocity components from the various laser beams are extracted by a straight forward geometrical regression.[8] The temperatures associated with each component are elliptically related assuming statistical independence.[8] The velocity distributions were calculated via Eqn. 1 assuming Gaussian profiles about the bulk velocity. The energy distributions were calculated directly from the velocity distributions:

$$E[V] = \frac{m v_i^2}{2e} \qquad (2)$$

A detailed lineshape model was used to determine the temperature and Doppler shifts of the fluorescence signals.[8] Only Gaussian broadening was considered since the magnetic fields, Stark broadening, and natural line widths are negligibly small.

Emission Spectroscopy

Assuming an optically thin plasma and noting that the transmission function, $T(\lambda)$, is constant over the line widths of the emission spectra, the number density of state j, n_j, can be determined from the measured intensity given the transition probability, A_{ij},[9]

$$n_j = \frac{4\pi\lambda}{hc} \frac{I(\lambda)}{A_{ij} L T(\lambda)} \qquad (3)$$

where L is the length of interrogation in the plasma. The transition probabilities are known for several Xe I and Xe II states and some Mo and W states.[9,10] For some states, A_{ij} can be approximated given the relative line strengths S_2/S_1:

$$A_{ij,2} = A_{ij,1} \frac{g_{j,1}\lambda_1^3}{g_{j,2}\lambda_2^3} \frac{S_2}{S_1} \quad (4)$$

where g_j is the degeneracy of state j.[10]

An approximation of the plasma condition can be made in terms of the number density of the excited states assuming local thermodynamic equilibrium.[9] This assumption is not strictly valid, but the LIF line shapes are sufficiently close to convolutions of pure Gaussians to indicate that it is not unreasonable as a first approximation. The distribution of excited states is, then,

$$\frac{n_j}{n} = \frac{g_j \exp\left(-E_j / kT\right)}{Q_{el}} \quad (5)$$

where E_j is the energy of state j and Q_{el} is the electronic partition function.

Using distribution temperatures measured by LIF, three Boltzmann relations (Eqn. 5) and a conservation of atoms relation provide a closed set of equations for the total number density of each species and the distribution temperature.[9]

Sputtering

Sputtering of discharge chamber materials by low-energy ions (<100 V) has been the subject of much theoretical but little experimental investigation.[11] The erosion sputtering yield, $y(E,\theta)$, can be expressed as a function of ion energy, E, and angle from normal incidence, θ:

$$y(E,\theta) = y(E)\cos^{-\gamma}(\theta)\exp\left\{-\sigma(\cos^{-1}(\theta)-1)\right\} \quad (7)$$

where

$$y(E) = K\left(E - E_{TH}\right)^2$$

for small θ, or

for larger angles,

$$E_T = \frac{m_1 + m_2}{m_2} \frac{Z_1 Z_2 e^2}{a},$$

$$a = 0.4685\left(Z_1^{2/3} + Z_2^{2/3}\right)^{-1/2},$$

the subscripts 1 and 2 refer to the incident and target materials respectively, and K, γ, and σ are empirical constants.

The flux of atoms sputtered from the surface of the DCA can be calculated from the erosion rates given above for the 2000 hr wear-test. These are $2.55\ 10^{18}$ $m^{-2}s^{-1}$ and $4.98\ 10^{18}$ $m^{-2}s^{-1}$ for W and Mo, respectively. The number density of incident Xe II ions is given in Fig. 3 as a function of incident energy and angle. This density is based on the inverse sputter yield (ratio of incident Xe II ions to eroded atoms) and the velocity of the ions with the specified energy.

The effects of Th impregnation of the W have been neglected due to the uncertainty in the value of the resulting sublimation energy, E_S. The curves' upper limits correspond to the threshold energies. Note the significant decrease in flux required at lower energies for angles of incidence near 55 degrees. This would suggest a source of the erosion-causing high-energy ions roughly 0.5 cm downstream of the orifice.

Results and Discussion

Laser-Induced Fluorescence

Xe II velocities and temperatures were measured in the discharge chamber for several operating conditions. These conditions are summarized in Table 1. The 2000 hr wear-test was conducted almost entirely at the 2.3 kW condition. Typical 4-beam data are presented in Fig. 4. Note the close overlapping of the fluorescence spectra. This illustrates the sensitivity of the measurements to both the size and resolution of the angles of the beams. The uncertainty associated with the angles and in the fitting resulted in an error bound of roughly 10 percent.

Xe II velocities along the centerline downstream of the DCA are given in Fig. 5. Note that the velocity is negative just downstream of the cathode in the 1.5 and 2.3 kW cases. The velocities level off around 2 cm away from the cathode to about 2000 m/s for all cases. The negative to positive transition in the centerline velocities is consistent with a the presence of a potential-hill roughly located between 0.5 and 0.75 cm downstream of the cathode orifice. As seen in previous studies, this phenomenon appears more strongly at higher currents.[12,15]

The calculated velocity distributions just downstream of the orifice for the 1.0 kW and the 2.3 kW cases are given in Fig. 6. The corresponding energy distributions are given in Fig. 7 where, the energy is given a direction V/|V| in order to better illustrate what ion energies are striking the orifice plate. Note that the tail of the 2.3 kW distribution extends to –19 V (implying a small fraction of Xe II ions are moving upstream with an energy of 19 V). This tail implies that a sufficiently large portion of the total ion flux may be striking the orifice plate. At lower powers, the energy distribution was significantly narrower with full-widths at half maximum (FWHM's) on the order of 2 V as is illustrated by the 1 kW case. The trends in the axial ion velocities shown in Fig. 5 are comparable to

those observed downstream of a cathode operating at lower currents.[12] However, the peak velocities

Table 1: Discharge cathode operating conditions

Power (kW)	J_D (A)	V_D (V)	m_{DC} (sccm)	m_M (sccm)	V_S (V)
0.5	4.31	25.5	2.48	6.0	650
1.0	6.05	24.8	2.46	8.3	1100
1.5	8.24	25.9	2.47	14.5	1100
2.3	12.1	27.7	2.90	22.8	1100

are lower than previous investigations would lead one to expect.[12,15]

The energy distribution can be normalized by integrating over its entire range. The normalized energy distribution can then be integrated over the range of energies where sputtering might be expected. This yields the density fraction of ions with sufficient energy to erode the target metal, $n^+(E)$, of the total density of Xe II, n^+. This was done numerically. For Xe II direct impingement, the tail barley crosses the -19 V point yielding an $n^+(E)/n^+$ of roughly $1.4 \cdot 10^{-3}$. For doubly charged ions, the integral's limit increases to -10 V where the ratio becomes 0.234.

Ion temperatures are given in Fig. 8 for various locations and operating conditions. The temperature decreases with power implying a more spot-like mode. Consistent with this, the plume downstream of the cathode was observed to become less diffuse as the power was increased.

Xe I temperatures were measured in the discharge chamber 0.5 and 1 cm downstream of the DCA cathode orifice during 2.3 kW operation. The neutral temperature decreased from 2500 K to 1300 K. Resolving the temperature required significant neutral density filtering of the large background fluorescence. No Xe I data were obtained within 0.5 cm of the orifice. The combination of noise and filtering yielded and uncertainty of 15 percent in the neutral temperature measurements.

The Xe I temperatures measured in the discharge chamber were slightly higher than those measured at similar locations in the 6 A plume of a keepered cathode used in previous investigations.[12] Unfortunately, the temperature could not be measured within 0.5 mm of the DCA where very high temperatures might be expected. The downstream temperature of 2500 K is more consistent with plume-mode operation.

Emission Spectroscopy

Emission spectroscopy data were collected downstream of the cathode for several operating conditions yielding order-of-magnitude data on the xenon state populations. The data indicated a significant increase in the fraction of doubly charged ions with power. At 0.5 kW, n^{++}/n^+ is on the order of 0.01. At 1.5 and 2.3 kW the fractions are 0.05 and 0.10 respectively.

The total number density can be approximated given the cathode and main flow rates. The ionization fraction, n^+/n, was roughly eighteen percent in the plume of the cathode. This is somewhat higher than the nominal ten percent ionization fraction in the thruster, but probably results from the measurement being made in the cathode plume, the primary location of ionization. The Xe II number density was roughly $2.6 \cdot 10^{18}$ m^{-3} which is slightly lower than the density measured downstream of _" hollow cathode assembly (HCA) operating at a lower current with a similar flow rate and relatively comparable ambient pressure (10^{-4} Torr).[12]

Note that Xe III would have sufficient energy for erosion of the DAC given Figs. 3 and 7. The sputtering yield would be at least twice that of Xe II due to its higher energy, but might be up to four times as much because of secondary interactions at the surface.[11] Considering the combination of n^{++}/n^+ and $n^+(E)/n^+$ equal to 0.1 and 0.234 respectively, the equivalent Xe II number density of Xe III would be roughly $6 \cdot 10^{17}$ m^{-3} which is close to the predicted requirement in Fig. 3. Alternatively, the sputtering threshold for thorium impregnated tungston ,Th-W, may be as low as 13 V.[13] For a sputtering threshold of 13 V, the ratio $n^+(E)/n^+$ is on the order of 0.05 (yielding an $n^+(E)$ of roughly $1.3 \cdot 10^{18}$ m^{-3}). The curves of Fig. 3 would be shifted significantly to the left implying that the Xe II population itself may then contribute greatly to the erosion.

There were strong W, Mo, and Xe III emission lines within the first 0.5 cm downstream of the orifice. At 1.0 cm, the W and Mo signals were significantly lower though the Xe III lines remained strong. This would imply that the doubly charged ions were moving in bulk away from the orifice and/or that they were being created several millimeters downstream.

Cathode Oscillations

Oscillations in the discharge voltage and current were observed for all throttling conditions. The AC component of the discharge voltage was measured using an isolation transformer. A current probe measured the discharge current. The principal frequencies were 40 kHz and 1.15 MHz. The amplitudes of the oscillations decreased with thruster power, and the frequencies remained roughly constant. The magnitudes were inversely proportional to the discharge cathode flow rate at a given thruster power. For example, at the 2.3 kW operating condition, the discharge voltage oscillated ± 4.5 V at a flow rate of 3.5 sccm and ± 5.5 V at 2.75 sccm.

The cathode oscillations observed above were much weaker than those observed in previous plume mode operation where the voltage swings were as

much as 100 percent of the nominal discharge voltage.[13] They were, however, consistent with high current cathode phenomena.[14] While these fluctuations would not produce the high energy ions observed downstream of the cathode in other investigations, the ±4 V swings may have been sufficient to induce low energy sputtering, particularly with Xe III.

Conclusions

The measured upstream flux of Xe II towards the DCA orifice pate may not be sufficient to account for the erosion observed in the NSTAR wear tests. However, when coupled with a significant fraction of Xe III, which may have the same trends in energy and velocity distribution as the Xe II measured here, and fluctuations on the order of 25 percent of the discharge voltage the mechanisms were present to provide an ion flux large enough to erode the orifice plate at the observed rates. If indeed the Th impregnation of the W lowers the sputtering threshold by a factor of three, the measured Xe II flux itself might be sufficient.

A real-time UV LIF erosion rate measurement capability is being developed. In addition to being able to detect the densities of eroded W and Mo for various thruster and DCA operating conditions, Xe III velocities may also be mapped. In addition, visible LIF will be used to more closely resolve the location of a potential hill if it exits. A low energy, calibrated ion source may be used in conjunction with these measurements to provide absolute (in addition to relative) erosion rate measurements.

Acknowledgements

This work was made possible by the continuing support of NASA GRC and the personnel associated with the On-Board Propulsion Branch, especially M. Patterson. The research has been conducted under NASA grants NAG-31572 and NAG-32216 monitored by J. Sovey.

The authors would like to thank the Department's technicians and the other students in the PEPL group for their assistance and support.

References

[1] Patterson, M. J., et al, "2.3 kW Ion Thruster Wear Test," AIAA-95-2516, 31st Joint Propulsion Conference (July, 1995).

[2] Polk, J. E., et al, "A 1000-Hour Wear Test of the NASA NSTAR Ion Thruster," AIAA-96-2717, 32nd Joint Propulsion Conference (July, 1996).

[3] Polk, J. E., "An Overview of the Results from an 8200 Hour Wear Test of the NSTAR Ion Thruster," AIAA-99-2446, 35th Joint Propulsion Conference (June, 1999).

[4] Brophy, J. R., et al, "The Ion Propulsion System on NASA's Space Technology 4/Champollion Comet Rendezvous Mission," AIAA-99-2856, 35th Joint Propulsion Conference (June, 1999).

[5] Domonkos, M. T., "Evaluation of Low-Current Orificed Hollow Cathodes," Ph.D. Thesis, The University of Michigan, October, 1999, pp 153-157.

[6] Katz, I., and Patterson, M. J., "Optimizing Plasma Contactors for Electrodynamic Tether Missions," Presented at Tether technology Interchange, September 9, 1997, Huntsville, AL.

[7] Kameyama, I., and P. J. Wilbur, "Potential-Hill Model of High-Energy Ion Production Near High-Current Hollow Cathodes," ISTS-98-Aa2-17, 21st International Symposium on Space Technology and Science, (May, 1998).

[8] Williams, G. J., et al, "Laser Induced Fluorescence Measurement of the Ion Velocity Distribution in the Plume of a Hall Thruster," AIAA-99-2424, 35th Joint Propulsion conference (June, 1999).

[9] Manzella, D. H., "Stationary Plasma Thruster Plume Emissions," IEPC-93-097, 23rd International Electric Propulsion Conference (September, 1993).

[10] Lide, D. R., Editor-in-Chief, CRC Handbook of Physics and Chemistry: 73rd Edition, CRC Press, Boca Raton, 1992.

[11] Duchemin, O. B., et al, "A Review of Low Energy Sputtering Theory and Experiments," IEPC-97-068, 25th International Electric Propulsion Conference (September, 1997).

[12] Williams, G. J., et al, "Laser Induced Fluorescence Characterization of Ions Emitted from Hollow Cathodes," AIAA-99-2862 (June, 1999).

[13] Morgulis, N. D., and V. D. Tishchenko, "The Investigation of Cathode Sputtering Near Threshold Region I," Soviet Physics JETP, **3** (1) August, 1956, 52-56.

[14] Domonkos, M. T., et al, "Low Current Hollow Cathode Evaluation," AIAA-99-2575, 35th Joint Propulsion Conference (June, 1999).

[15] Friedly, V. J., and P. J. Wilbur, "High Current Hollow Cathode Phenomena," Journal of Propulsion and Power, **8** (3) May-June, 1992, 635-643.

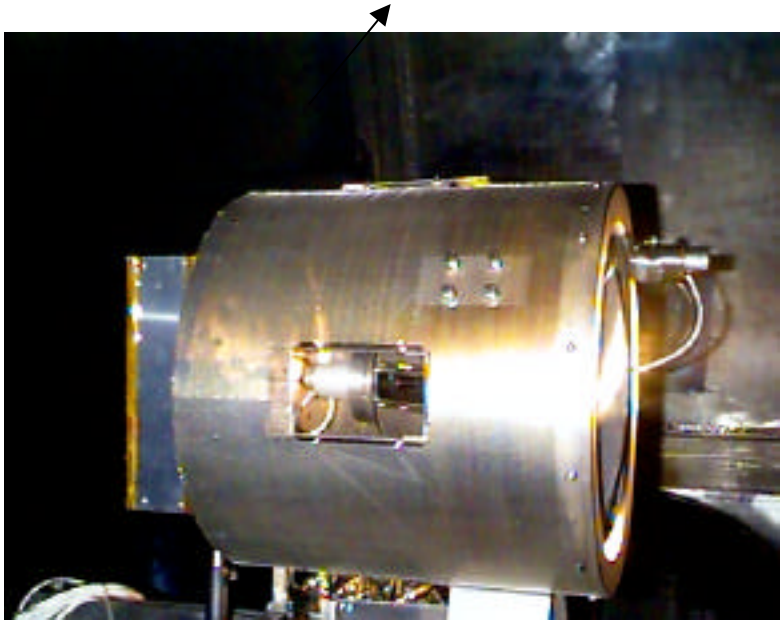

Fig. 1 A photograph of the 30 cm FMT-2 ion engine showing the location of the quartz windows. The windows are located at 0, 90, and 180 degrees

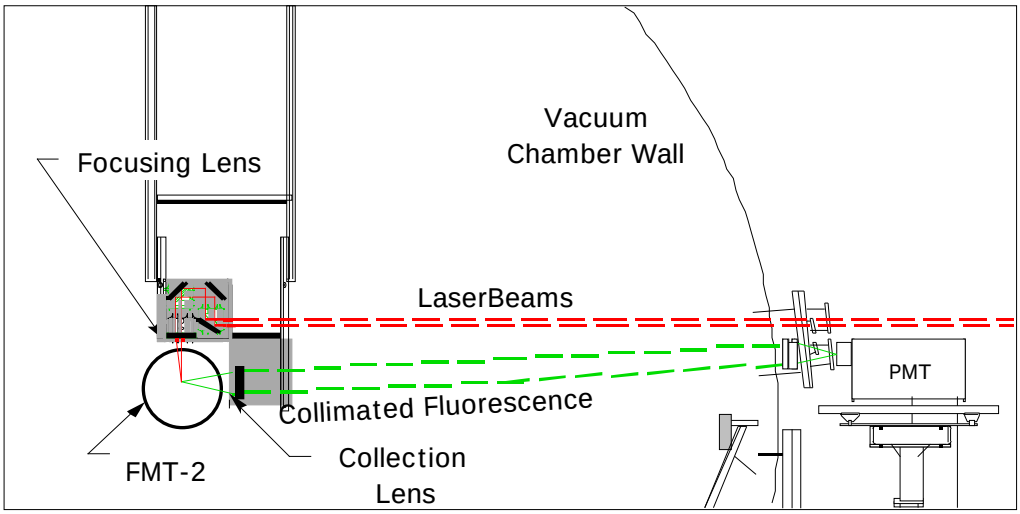

Fig. 2 A schematic of the laser delivery and fluorescence collection optics. This is not to scale

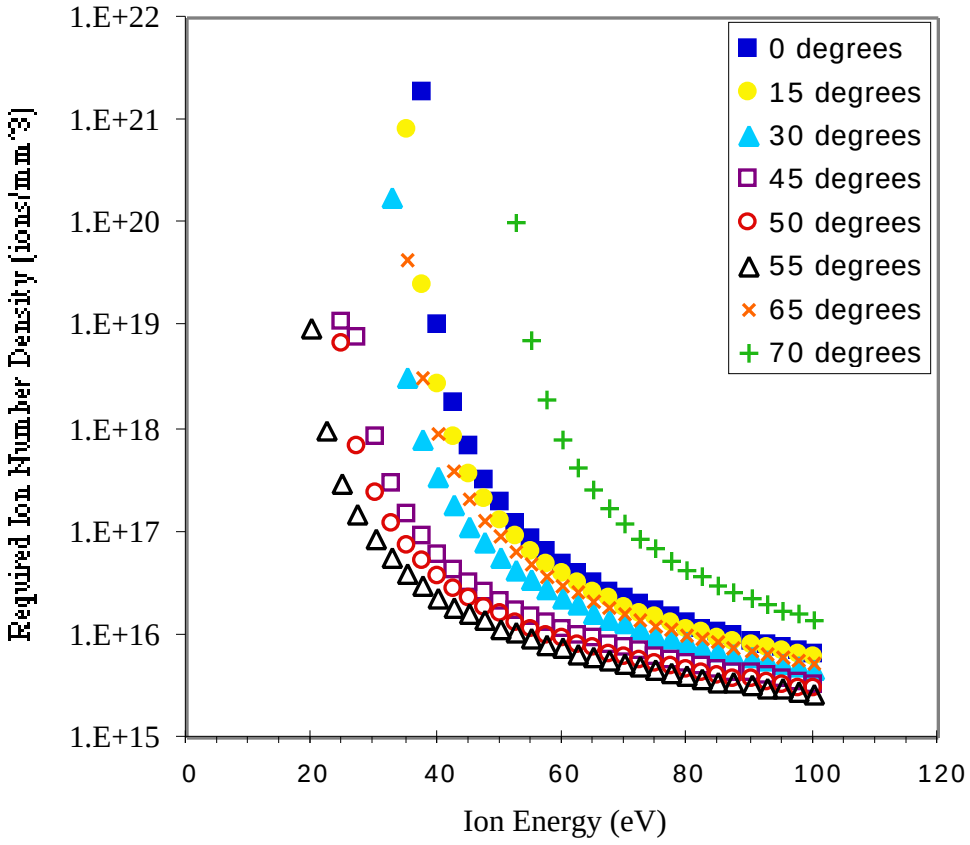

Fig. 3 Xe II number density required to achieve observed W erosion on the 2000 hr DCA's. The curves for Mo erosion are similar.

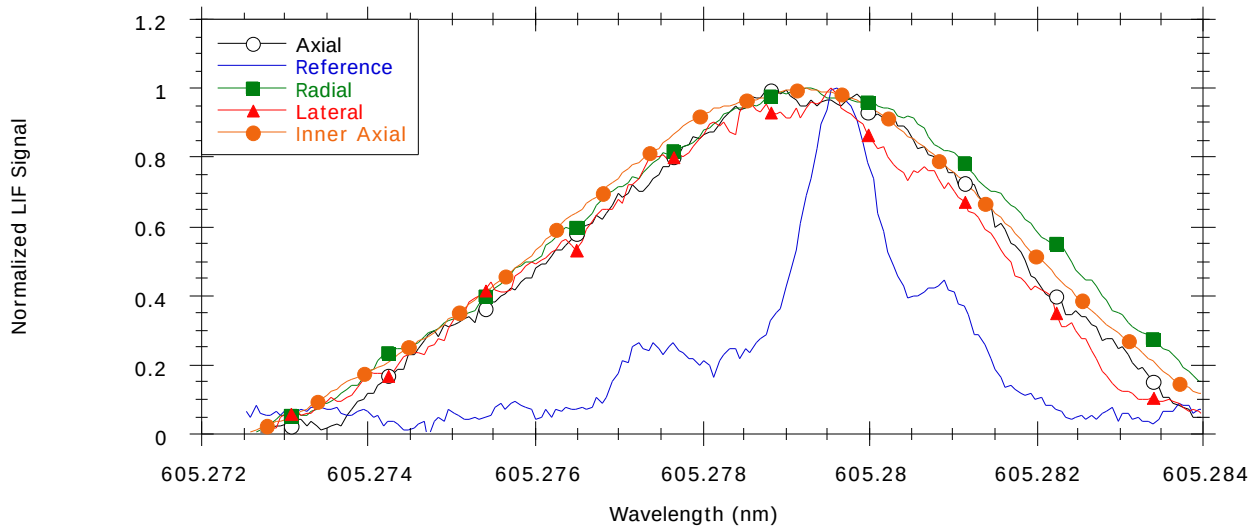

Fig. 4 Typical 4-beam LIF signals in the DCA plume. Note the close spacing.

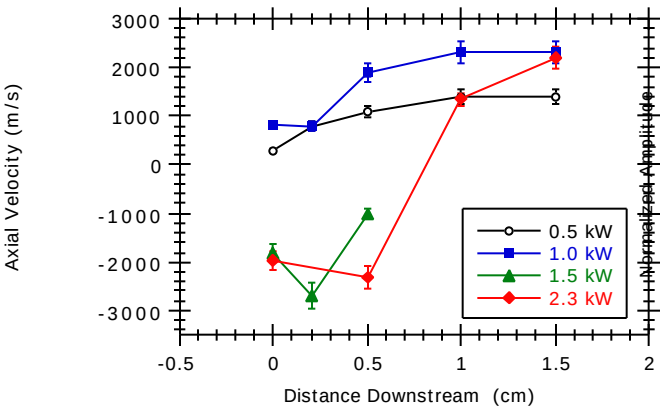

Fig. 5 Axial Xe II velocities for various thruster powers.

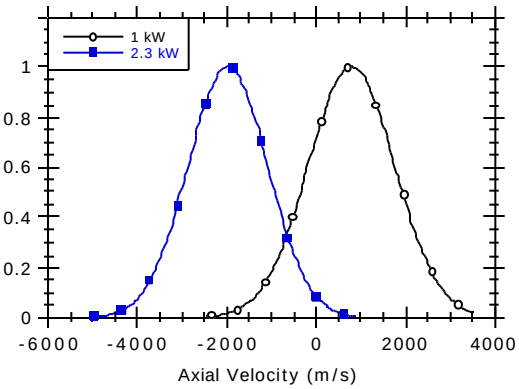

Fig. 6 Axial Xe II velocity profiles for 1.0 and 2.3 kW operation

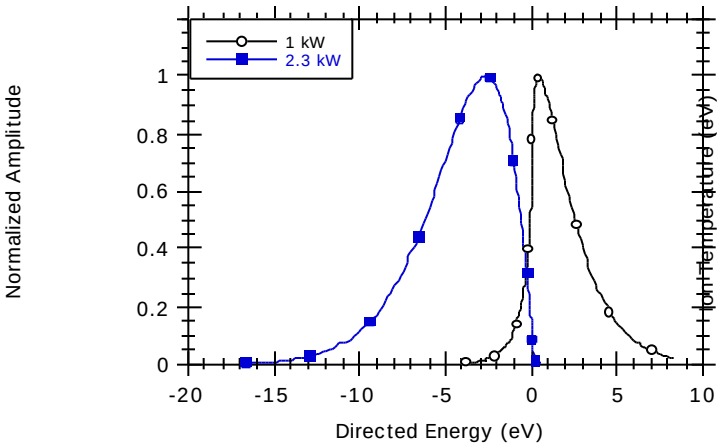

Fig. 7 Axial Xe II directed energy distributions for 1 and 2.3 kW operation

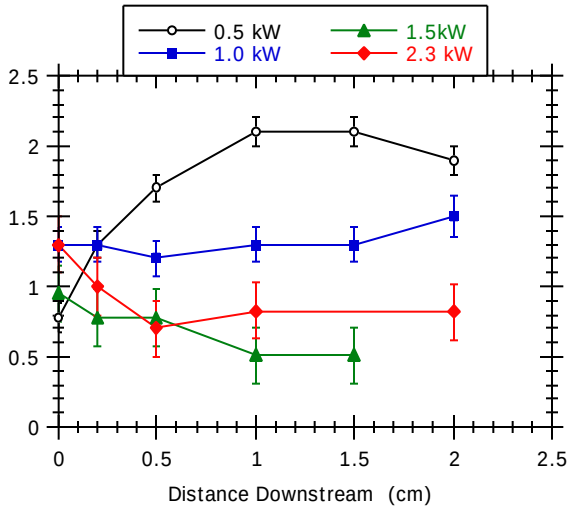

Fig. 8 Axial temperatures for various thruster powers.